coatings

MDPI

Article

One-Dimensional CdS/$SrTiO_3$/Carbon Fiber Core–Shell Photocatalysts for Enhanced Photocatalytic Hydrogen Evolution

Qi Hu [1,2], Jiantao Niu [3], Ke-Qin Zhang [1,*] and Mu Yao [4]

[1] National Engineering Laboratory for Modern Silk, College of Textile and Clothing Engineering, Soochow University, Suzhou 215123, China
[2] School of Social Development and Public Administration, Suzhou University of Science and Technology, Suzhou 215009, China
[3] School of Textile and Clothing and Arts and Media, Suzhou Institute of Trade and Commerce, Suzhou 215009, China
[4] School of Textile Science and Engineering, Xi'an Polytechnic University, Xi'an 710048, China
* Correspondence: kqzhang@suda.edu.cn; Tel.: +86-512-67061169

Abstract: The photocatalytic hydrogen production efficiency of a single $SrTiO_3$ photocatalytic catalyst is often low, which is mainly due to the serious combination of electrons and holes produced by photocatalysis as well as the mismatch of the redox capacity and light absorption range. Construction of semiconductor heterojunctions can solve these problems. CdS has a narrow band gap, which can effectively utilize visible light, and it has a band structure matched with that of $SrTiO_3$. Therefore, CdS is considered as an ideal candidate for constructing heterojunctions with $SrTiO_3$. In this paper, bamboo pulp fibers were used as the substrate, and $SrTiO_3$ was coated on the substrate through the solvothermal process. CF/$SrTiO_3$ rich in oxygen vacancies was formed by high temperature carbonization, and heterojunctions were formed by loading CdS on the surface of the CF/$SrTiO_3$ composite material through the hydrothermal method, thus obtaining one-dimensional CF/$SrTiO_3$/CdS core–shell photocatalysts. The structure and photocatalytic hydrogen production performance of the CF/$SrTiO_3$/CdS core–shell photocatalysts were mainly studied. The photocatalytic hydrogen production experiment showed that the hydrogen production rate of the CF/$SrTiO_3$/CdS-2 sample under the optimized process was as high as 577.39 μmol/g·h, which was about 11 times that of the CF/$SrTiO_3$ sample. In this composite photocatalytic material system, the loading of the CdS nanospheres could enhance the visible light absorption capacity of the composite catalyst, promote the rapid separation and high-speed migration of photocarriers, and significantly improve the photocatalytic activity.

Keywords: $SrTiO_3$; photocatalytic; hydrogen production; carbon fiber; oxygen vacancy; CdS

Citation: Hu, Q.; Niu, J.; Zhang, K.-Q.; Yao, M. One-Dimensional CdS/$SrTiO_3$/Carbon Fiber Core–Shell Photocatalysts for Enhanced Photocatalytic Hydrogen Evolution. *Coatings* **2022**, *12*, 1235. https://doi.org/10.3390/coatings12091235

Academic Editor: Alexandru Enesca

Received: 2 August 2022
Accepted: 22 August 2022
Published: 24 August 2022

1. Introduction

Photocatalytic hydrogen production can not only produce highly efficient and clean hydrogen energy using clean and renewable solar energy, but it also requires simple equipment and mild reaction conditions and has low cost, which is the most attractive method for hydrogen production. The key to improving the efficiency of photocatalytic hydrogen production is to develop efficient and stable photocatalysts. Because of the excellent redox catalytic activity and environmental friendliness, $SrTiO_3$ exhibits many intriguing properties that make it a good candidate for potential applications in a wide array of fields, which include water splitting, sewage treatment, air purification, and virus inactivation [1]. To produce efficient photocatalytic performance, the materials should possess high mobility carriers, suitable band gap width, and higher absorption capacity [2]. However, the wide band gap makes $SrTiO_3$ photocatalysts only respond to ultraviolet light, so pure $SrTiO_3$ normally exhibits mediocre photocatalytic activity because of its limited surface-active sites and fast recombination of the photoexcited electron–hole pairs. Various methods have therefore been proposed to address these issues, such as dopant

introduction [3], heterojunction construction [4,5], loading precious metal [6], surface defect modification [7], surface decorating with 2D materials [8], and building sundry nanoarchitectures. Specifically, heterojunction construction has been proven to be one of the best methods to improve photocatalytic performance, and it is the most effective method with the most potential for practical application because of its feasibility and efficiency for the spatial separation of electron–hole pairs [9]. This paper focuses on the construction of heterojunctions to improve the photocatalytic activity of $SrTiO_3$.

By virtue of its narrow bandgap (~2.4 eV) [10,11] and favorable band position, CdS has been widely explored as a photocatalyst for solar hydrogen generation. Previous studies on CdS-based photocatalysts mainly focused on the design of Janus-type nanostructures [12], core–shell nanostructures [13], hollow nanostructures [14], and surface-decorated heterostructure [15]. There are many reports about the heterojunction construction of CdS [16–18], but CdS composite photocatalyst loading on carbon fiber (CF) is scarcely studied. CdS has a band structure matched with that of $SrTiO_3$. Therefore, CdS is considered as an ideal candidate for constructing heterojunctions with $SrTiO_3$. When CdS and $SrTiO_3$ are compounded, they have a synergistic effect in photocatalytic reaction. In addition, both semiconductor materials have a strong photocatalytic capacity, which is beneficial to accelerate the photocatalytic reaction rate and improve the efficiency of hydrogen production.

Bamboo pulp fiber is a relatively fine cellulose fiber, which contains a large number of hydroxyl groups and grooves on the surface. It is easy to load the photocatalytic semiconductor material onto the surface of the bamboo pulp fiber during the solvothermal process. Moreover, bamboo pulp fiber can be carbonized into carbon fiber at high temperature. In this work, bamboo pulp fiber was used as a substrate, $SrTiO_3$ was coated on the surface of the substrate through the solvothermal process, and carbon fiber/$SrTiO_3$ (CF/$SrTiO_3$) rich in oxygen vacancies was formed by high temperature carbonization. Heterojunctions were formed by loading CdS on the surface of the CF/$SrTiO_3$ through the hydrothermal method to thus prepare one-dimensional CF/$SrTiO_3$/CdS core–shell photocatalysts, and the structure and photocatalytic hydrogen production performance of the CF/$SrTiO_3$/CdS core–shell photocatalysts were mainly studied.

2. Experimental

2.1. Materials

Strontium acetate ($C_4H_6O_4Sr$, 99%), cadmium acetate ($C_4H_6CdO_4{\cdot}2H_2O$, 99%), and thiourea (CH_4N_2S, 99%) were purchased from Aladdin Reagent Co., Ltd. (Shanghai, China). Titanium (IV) isopropoxide ($C_{12}H_{28}O_4Ti$, 97%) was from Macklin Co., Shanghai, China. Ethanol and ethylene glycol were from Sinopharm Chemical Reagent Co., Ltd., China. All the chemical reagents were of analytically pure grade and used as received without any purification.

2.2. Preparation of CF/$SrTiO_3$/CdS Composite Material

In this work, firstly, bamboo pulp fiber (Hebei Jigao Chenical Fiber Co., Ltd., Shijiazhuang, China) was used as the precursor of carbon fiber, and the $SrTiO_3$ nanolayer was loaded onto the surface of the bamboo pulp fiber, and then carbon fiber was carbonized to prepare CF/$SrTiO_3$ core–shell composite fiber material. Finally, the CF/$SrTiO_3$/CdS double-layer core–shell photocatalytic composite fiber material was prepared by loading CdS on CF/$SrTiO_3$ composite fiber [19,20]. The specific preparation process is shown in Scheme 1.

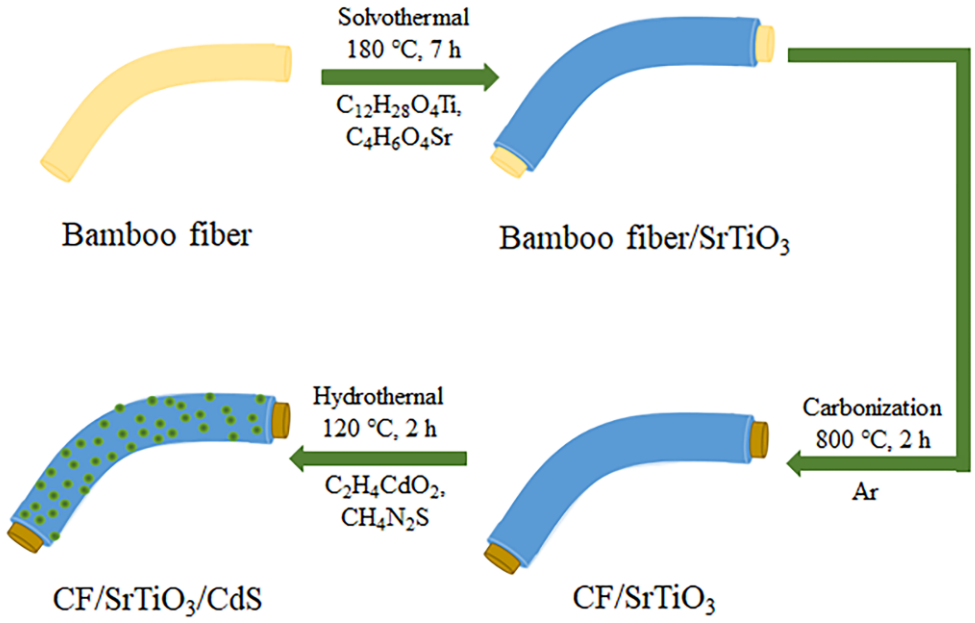

Scheme 1. Flow chart for preparing CF/$SrTiO_3$/CdS double-layer core–shell structure heterojunctions.

2.2.1. Preparation of Bamboo Fiber/$SrTiO_3$ Composite Fiber

The $SrTiO_3$ nanosemiconductor material was coated on the bamboo pulp fiber through the solvothermal process. First, 19 mL of absolute ethyl alcohol and 15 mL of ethylene glycol were added separately to the beaker and mixed with adequate stirring. Then 0.85 g of titanium (IV) isopropoxide and 0.61 g of strontium acetate were added to the mixed solution and stirred adequately to obtain a homogeneous mixed solution. The above mixed solution was transferred to a PTFE reactor, 0.8 g of bamboo pulp fibers was added for impregnation, and the solvothermal reaction was carried out. The reaction temperature was kept at 180 °C, and the reaction time was 18 h. Following finish of the reaction and cooling to room temperature, the bamboo pulp fibers samples were draw out and rinsed with ethyl alcohol. The fiber samples were dried in a drying oven at 60 °C, thus obtaining the bamboo fiber/$SrTiO_3$ composite material. In this experiment, the solvent was a mixture of anhydrous ethanol and ethylene glycol without water, which could help to prevent the bamboo pulp fibers from dissolving.

2.2.2. Preparation of CF/$SrTiO_3$ Composite Fiber

CF/$SrTiO_3$ photocatalyst with a core–shell structure was prepared by carbonization of cellulose fibers. The bamboo fiber/$SrTiO_3$ composite material was prepared in a high-temperature tubular furnace by carbonizing cellulose fibers under the protection of an 800 °C argon atmosphere system for 2 h with a heating rate of 5 °C min. As the bamboo pulp fiber was converted into carbon fiber, the core–shell structured CF/$SrTiO_3$ photocatalyst was achieved, and the surface of the carbon fiber was coated with $SrTiO_3$ rich in oxygen vacancies.

2.2.3. Preparation of CF/$SrTiO_3$/CdS Composite Fiber

CF/$SrTiO_3$/CdS double-layer core–shell structure heterojunctions were prepared by the hydrothermal method. First, 50 mg, 100 mg, and 150 mg of cadmium acetate were respectively weighed and added to 35 mL of deionized water, and then 35 mg, 70 mg, and 100 mg of thiourea were respectively added [21]. The solution was transferred to the PTFE reactor after being stirred for 30 min and immersed in 0.07 g of CF/$SrTiO_3$ photocatalytic material. Subsequently, the PTFE reactor was transferred to the oven, and the hydrothermal reaction was carried out at 120 °C for 2 h. After the hydrothermal reaction was over, the carbon fiber composite material was drawn out and rinsed with ethyl

alcohol. The fiber samples were dried in the drying oven at 60 °C for 24 h, thus yielding the CF/$SrTiO_3$/CdS double-layer core–shell structure heterojunctions [22]. In this process, the above samples with different proportions were respectively labeled as CF/$SrTiO_3$/CdS-1, CF/$SrTiO_3$/CdS-2, and CF/$SrTiO_3$/CdS-3.

According to the test needs, pure $SrTiO_3$ and CdS samples as well as carbon fiber samples were prepared by referring to the above methods.

2.3. Characterization Method

The crystalline structures of the samples were characterized by an X-ray diffractometer (XRD, Bruker D8 Discover, Billerica, MA, USA). The morphologies of the as-prepared products were characterized by an electron microscope (FESEM Hitachi S-4800, Tokyo, Japan) and a transmission electron microscope (TEM FEI talos F200x G2, Philips-FEI Corpocyclen, Eindhoven, The Netherlands). X-ray photoelectron spectroscopy (XPS) measurements were performed on a Thermo ESCALAB 250XI (Thermo Fisher Scientific, Fairport, NY, USA), and the defects of the samples were tested and characterized by an electronic paramagnetic spectrometer (EPR, Bruker A300, Billerica, MA, USA). The electrochemical impedance and Mott–Schottky curve of the samples were tested by an electrochemical workstation (CHI660E, YIMA, Shanghai, China) with the standard three-electrode testing method. The UV–vis diffuse reflectance spectra (DRS) were performed on a Hitachi F-7000 spectrophotometer (Hitachi, Fukuoka, Japan). The specific surface area of the catalysts was calculated using the Brunauer–Emmett–Teller (BET, Bruker A300, Billerica, MA, USA) equation.

2.4. Test of Photocatalytic Hydrogen Production Performance

The photocatalytic hydrogen production performance of the samples was tested by the Labsolar III system (Beijing Perfectlight Technology Co. Ltd., Beijing, China) [23], including a gas chromatography (GC-7900, Tianmei, Shanghai, China). An external irradiation type photocatalytic reactor with 150 mL volume was used, which was connected to a closed gas circulation and evacuation system. High purity AR was used as the carrier gas, and the gas chromatography (GC-7900) equipped with a TCD detector and 5 Å molecular sieve column was used to analyze the evolved H_2 gas. Before the experiment, 100 mg of catalyst sample was added into the mixture of 50 mL of Na_2S (0.35 M) solution and 50 mL of Na_2SO_3 (0.25 M) solution, wherein Na_2S and Na_2SO_3 were used as sacrificial agents in the photocatalytic hydrogen production experiment [24,25]. Prior to the irradiation test, the reactant solution was evacuated several times to remove air. The solution was added to the photocatalytic reactor and stirred by magnetic force. During the experiment, a plS-SE300C 300 W arc lamp (Beijing perfectlight Co., Ltd., Beijing, China) was used to simulate the solar light source for testing, and the light source intensity was 100 mW/cm^2. The water in the photocatalytic reactor with an external cooling coil was cooled to keep the mixture temperature at about 25 °C.

3. Experimental Result and Analysis

The phase structure of the catalyst can be analyzed through X-ray crystal diffraction. The XRD energy spectra of the samples such as CF/$SrTiO_3$/CdS, CF/$SrTiO_3$, CF, $SrTiO_3$, and CdS are each exhibited in Figure 1. The characteristic diffraction peaks of the pure $SrTiO_3$ sample were mainly distributed at 32.4°, 39.9°, 46.5°, 57.8°, 67.8°, and 77.1°, which can be respectively identified as the (110), (111), (200), (211), (220), and (310) crystal faces (PDF#35-0734) [26,27]. Compared with the characteristic diffraction peak energy spectrum of the pure $SrTiO_3$ sample, the shapes and positions of distinctive characteristic diffraction peaks in the XRD energy spectra of the CF/$SrTiO_3$ and CF/$SrTiO_3$/CdS samples were similar to those of the pure $SrTiO_3$, indicating that $SrTiO_3$ was coated smoothly on these carbon fibers. The XRD energy spectrum of CF formed by carbonization of bamboo pulp fibers showed only one broad carbon diffraction peak, indicating that the carbon fibers have an amorphous structure [28,29], and therefore the corresponding carbon diffraction

peaks in the XRD energy spectra of CF/$SrTiO_3$ and CF/$SrTiO_3$ materials were not obvious. The pure CdS sample had obvious diffraction peaks at 24.8°, 26.4°, 28.1°, 43.9°, 47.9°, and 52.0°, respectively belonging to (100), (002), (101), (110), (103), and (112) crystal faces in accordance with PDF#41-1049. It could be observed from the XRD energy spectrum of the CF/$SrTiO_3$/CdS sample that there were not only characteristic diffraction peaks attributed to $SrTiO_3$, but also obvious diffraction peaks at 26.4°, 43.9°, and 52.1°, which could be attributed to CdS characteristic diffraction peaks (PDF#41-1049) [30]. This indicated that the $SrTiO_3$ and CdS semiconductor materials were successfully loaded onto the surface of CF.

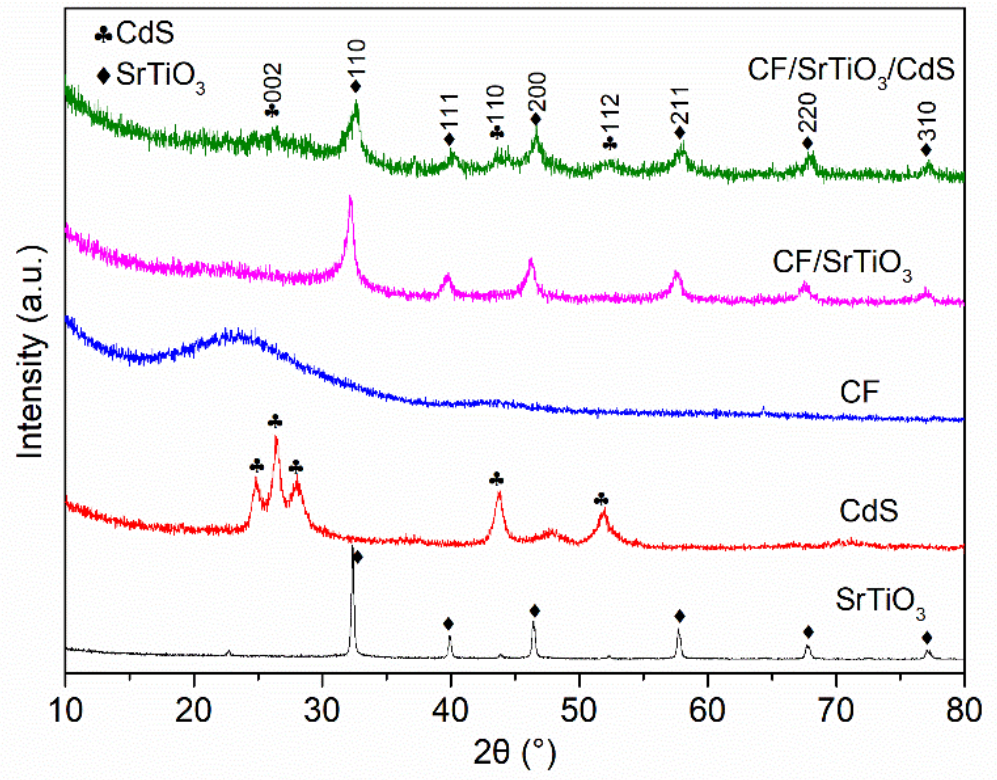

Figure 1. XRD energy spectra of samples.

The microscopic morphologies of CF/$SrTiO_3$/CdS, CF/$SrTiO_3$, and pure carbon fiber were characterized by the SEM test, and the results are exhibited in Figure 2. These carbon fibers prepared from bamboo pulp fibers were elongated soft fibers with smooth surfaces and grooves [31], and the fiber diameter was about 5 μm (Figure 2a) [32]. It can be seen from Figure 2b that $SrTiO_3$ nanoparticles were grown on the surface of each carbon fiber with relatively uniform distribution. As shown in Figure 2c, the coating layer was formed by $SrTiO_3$ nanoparticles on the surface of each carbon fiber with core–shell structures, and the $SrTiO_3$ material was integrated with the carbon fibers with compact structures. The $SrTiO_3$ material was irregular nanoparticles with a size of 100–200 nm. Figure 2d–f show an SEM diagram of the CF/$SrTiO_3$/CdS composite catalyst with different magnification factors, from which it can be observed that CF/$SrTiO_3$/CdS had a complete morphology and a uniform thickness. CdS nanospheres were coated on the outer layer of CF/$SrTiO_3$ to form a double-layer core–shell structured photocatalyst. As seen in Figure 2f, the CdS nanospheres were assembled and sedimented on the outer layer of CF/$SrTiO_3$, and the size of the CdS nanospheres was about 80 nm.

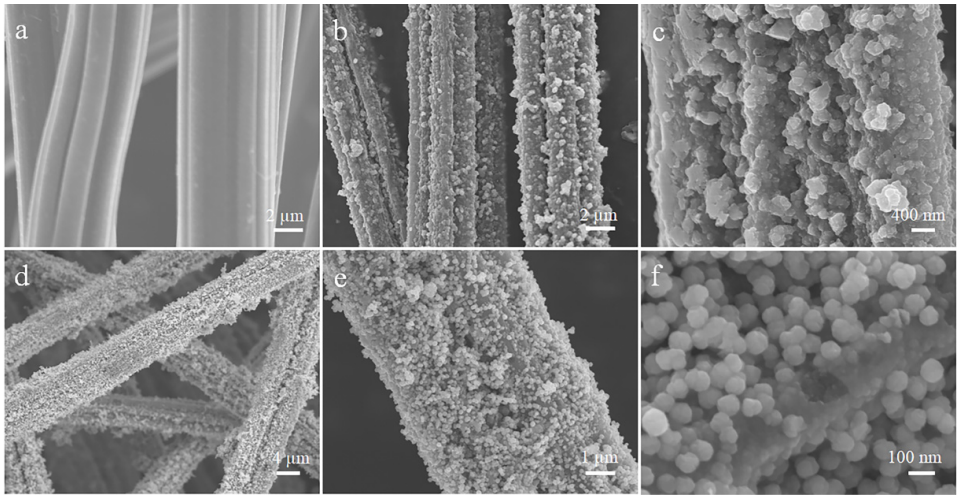

Figure 2. SEM diagram of samples: (**a**) carbon fiber (CF), (**b**,**c**) CF/$SrTiO_3$, (**d**–**f**) CF/$SrTiO_3$/CdS.

The element distribution of CF/$SrTiO_3$/CdS was studied by SEM mapping, as shown in Figure 3. SEM mapping was mainly used to study the element distribution over the surface of the CF/$SrTiO_3$/CdS photocatalytic composite fibers, but carbon fibers were located in the center of the CF/$SrTiO_3$/CdS core–shell structure. Therefore, as shown in Figure 3, relatively little carbon element was detected in the CF/$SrTiO_3$/CdS fiber [31]. It can also be seen in Figure 3 that Ti, Sr, O, Cd, and S elements were uniformly distributed on the surface of the carbon fibers. Combined with Figures 1 and 2, it can be determined that the preparation of CF/$SrTiO_3$/CdS was successful, and $SrTiO_3$ and CdS were evenly distributed on the carbon fibers.

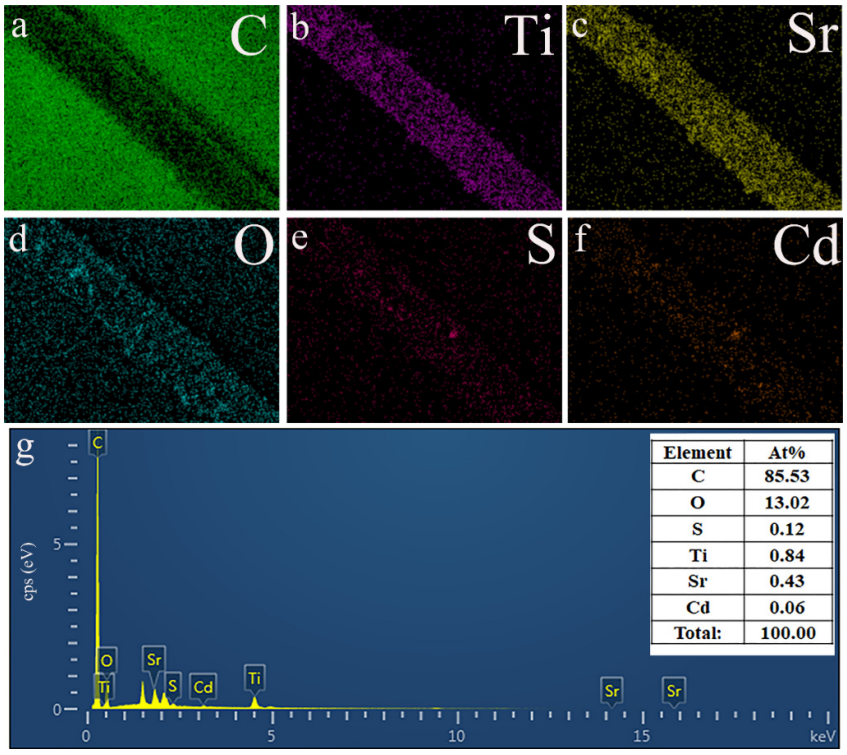

Figure 3. Element distribution of CF/$SrTiO_3$/CdS photocatalytic fiber: (**a**) C element, (**b**) Ti element, (**c**) Sr element, (**d**) O element, (**e**) S element, (**f**) Cd element, and (**g**) element content diagram of CF/$SrTiO_3$/CdS.

Qualitative analysis and element valence analysis of surface elements of the CF/$SrTiO_3$/CdS can be conducted by light ray photoelectron spectroscopy. A survey spectrum of the CF/$SrTiO_3$/CdS and high resolution XPS spectra of C 1s, Sr 3d, Ti 2p, Cd 3d, S 2p, and O 1s are shown in Figure 4. Figure 4a shows an XPS full spectrum of the samples, confirming that there were mainly six elements (i.e., Sr, Ti, Cd, S, O, and C) on the surface of the CF/$SrTiO_3$/CdS. Although the content of carbon element was high, the signal of the carbon element shown in the figure was moderate, which was mainly because the carbon fibers were located in the center of the CF/$SrTiO_3$/CdS core–shell structure, while the signal of the Cd element was the strongest because the CdS nanospheres were coated on the CF/$SrTiO_3$ photocatalytic fibers. As seen in Figure 4b, it could be presumed from the spectrum of C 1s that the three fitting peaks at the binding energies of 284.7 eV, 285.6 eV, and 288.1 eV were, respectively, corresponding to C–C bonds, C–O bonds, and C=O bonds [33]. Combined with the XRD energy spectra (Figure 1), it was analyzed and presumed that the carbon fibers mainly have an amorphous structure that was similar to the structure of graphite. As seen in Figure 4c, Ti 2P had two peaks, namely, the Ti $2p_{3/2}$ peak at the binding energy of 459.2 eV and the Ti $2p_{1/2}$ peak at the binding energy of 464.9 eV (the difference between the Ti $2p_{3/2}$ peak and the Ti $2p_{1/2}$ peak was 5.7 eV), both corresponding to Ti–O bonds, and the Ti ion valence was +4 [34]. As shown in Figure 4d, Sr 3d also had two peaks, namely, the Sr $3d_{5/2}$ peak at the binding energy of 133.8 eV and the Sr $3d_{3/2}$ peak at the binding energy of 135.5 eV, both corresponding to Sr–O bonds, and the Sr ion valence was +2 [35]. It can be seen in Figure 4e that the spectrum of O 1s was fitted into three peaks, and it could be known after analysis that the peak at 530.4 eV corresponded to lattice oxygen in the photocatalyst, while the peak at 531.8 eV could be ascribed to the surface adsorption oxygen, and the peak at 532.6 eV corresponded to adsorption oxygen in oxygen vacancies [36]. The results indicated that there were oxygen vacancies in the CF/$SrTiO_3$/CdS, which was speculated to be due to the occurrence of oxygen defects in CF/$SrTiO_3$ during the carbonization process of bamboo pulp fiber coated with $SrTiO_3$ at high temperature [37]. In Figure 4f, S 2p had two peaks, namely, the S $2p_{3/2}$ peak at the binding energy of 162.1 eV and the S $2p_{1/2}$ peak at the binding energy of 163.3 eV, and the difference between the two peaks was 1.2 eV [38]. Figure 4g shows a high resolution XPS spectrum of Cd 3d. The two fitting peaks at the binding energies of 405.7 eV and 412.4 eV corresponded to Cd $3d_{5/2}$ and Cd $3d_{3/2}$ of Cd^{2+}, respectively, the difference value between these two peaks was 6.7 eV, and both peaks were corresponding to Cd–S bonds [39].

In order to deeply confirm the existence of oxygen vacancies of $SrTiO_3$ material, EPR testing was performed for CF/$SrTiO_3$ (Figure 5). There was a strong single peak at $g \approx 2.002$, explaining that oxygen vacancies existed in the CF/$SrTiO_3$ catalyst material, which may be caused by the $SrTiO_3$ material being loaded and oxygen vacancies being formed in the high temperature carbonization process of the bamboo pulp fibers [40,41]. The existence of the oxygen vacancies was beneficial to the absorption of visible light by the photocatalyst and the improvement of the charge transfer ability of the CF/$SrTiO_3$/CdS material.

The specific surface area and internal pore size of CF/$SrTiO_3$/CdS composite material were measured by the BET nitrogen adsorption volume method [42]. As shown in Figure 6a, it could be obtained by a BET calculation model that the specific surface area of the CF/$SrTiO_3$/CdS photocatalytic fiber was 75.34 cm^2/g, and it was calculated from a Barrett–Joyner–Halenda (BJH) equation that the average pore size of CF/$SrTiO_3$/CdS was about 2.148 nm, as shown in Figure 6b. The loading of the CdS nanospheres on the surface of the CF/$SrTiO_3$/CdS composite fiber was beneficial to improving the photocatalytic performance.

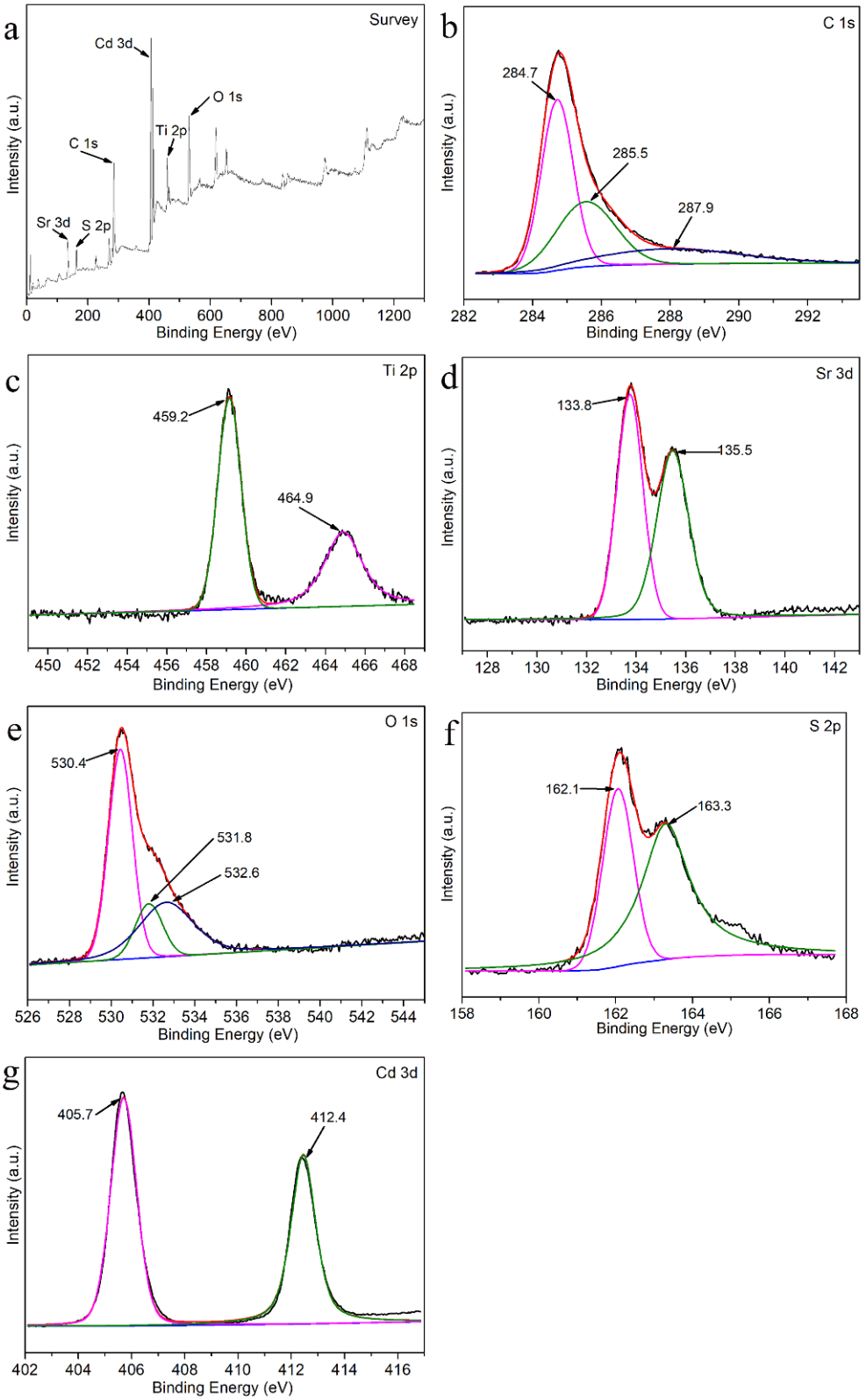

Figure 4. XPS spectra of CF/$SrTiO_3$/CdS: (**a**) full spectrum, (**b**) C 1s spectrum, (**c**) Ti 2p spectrum, (**d**) Sr 3d spectrum, (**e**) O 1s spectrum, (**f**) S 2p spectrum, and (**g**) Cd 3d spectrum.

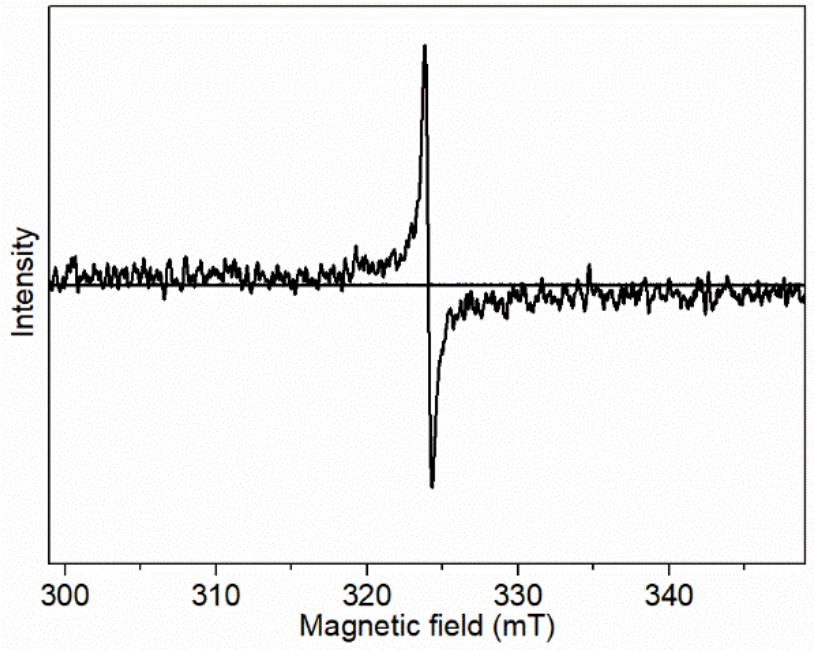

Figure 5. EPR oxygen vacancies of CF/$SrTiO_3$.

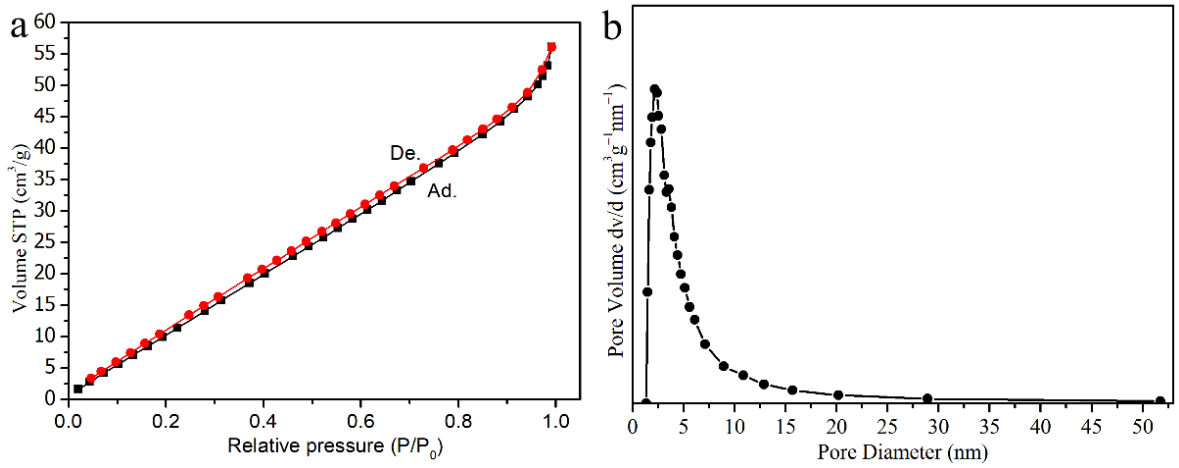

Figure 6. Nitrogen adsorption–desorption isothermal curve (**a**) and mesopore distribution (**b**) of CF/$SrTiO_3$/CdS.

CF/$SrTiO_3$/CdS is a fibrous catalyst with double-layer core–shell structure, and the central part of CF/$SrTiO_3$/CdS is carbon fiber, which is not semiconductor material and cannot be split into water to produce hydrogen under the action of light. As shown in Figure 7, the approximate content of $SrTiO_3$ and CdS in the CF/$SrTiO_3$/CdS composite material could be determined by the TG–DSC test [43]. It could be observed that a slow weight loss (about 5%) occurred between 40 °C and 360 °C, and this phenomenon may have been caused by the evaporation of water and the oxidation of CdS. Rapid decomposition occurred, and an obvious endothermic peak appeared between 360 °C and 510 °C, and the weight loss rate was as high as about 31%, which was presumed to be mainly caused by the oxidation and combustion of carbon fibers in air conditions. According to the above analysis, we can presume that the content of $SrTiO_3$ and CdS in CF/$SrTiO_3$/CdS was about 64%.

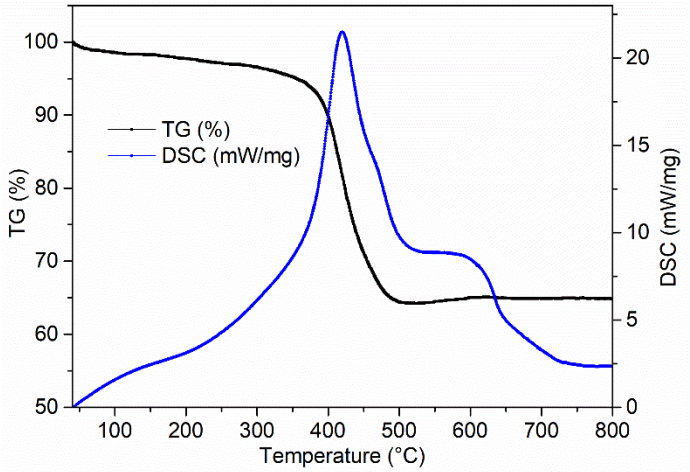

Figure 7. TG–DSC curve of CF/$SrTiO_3$/CdS.

To study the effect of CdS loading on the photocatalytic performance of CF/$SrTiO_3$, the photocatalytic hydrogen production performances of CF, CF/$SrTiO_3$, CF/$SrTiO_3$/CdS-1, CF/$SrTiO_3$/CdS-2, and CF/$SrTiO_3$/CdS-3 samples were tested, respectively (Figure 8). In the photocatalytic hydrogen production experiment, a 300 W xenon lamp was used for simulating solar light, and Na_2S and Na_2SO_3 were taken as corresponding sacrificial agents. The related data from Figure 8 indicated that carbon fibers alone had no hydrogen production evolution performance, while the photocatalytic hydrogen evolution of the CF/$SrTiO_3$ sample loaded with $SrTiO_3$ was about 53.27 μmol/g·h, which was close to that of pure $SrTiO_3$ (51.84 μmol/g·h) [44]. This was attributed to the fact that carbon fibers acted as a co-catalyst, and the synergistic effect of the oxygen vacancies and the carbon fibers promoted the separation and migration of the photoelectron–hole pairs, thus significantly improving the photocatalytic activity of the $SrTiO_3$ material. With the loading of CdS on the surface of CF/$SrTiO_3$, the photocatalytic hydrogen production was further improved. The hydrogen production rates of the CF/$SrTiO_3$/CdS-1 and CF/$SrTiO_3$/CdS-3 samples were, respectively, 211.96 μmol/g·h and 330.34 μmol/g·h, which were, respectively, about 4 times and 6.3 times that of the CF/$SrTiO_3$ sample. However, the hydrogen production rate of the CF/$SrTiO_3$/CdS-2 sample was as high as 577.39 μmol/g·h, which was about 11 times that of the CF/$SrTiO_3$ sample. This was mainly due to the much more efficient carrier utilization of compound photocatalyst caused by the increasing amount of CdS. Herein, the depressed performance of photocatalytic hydrogen generation was observed as the content of CdS was further increased from CF/$SrTiO_3$/CdS-3. This phenomenon was consistent with those found in the literature, where the photocatalytic efficiency of type-II nanoheterostructures declined as the constituent content exceeded the optimal value [45,46]. CdS is an excellent photocatalytic material for visible light, but under the condition of photoexcitation, the photogenerated carriers are easy to recombine, resulting in low quantum efficiency [47]. It was considered that with the increasing of CdS content, electron–hole recombination suppressed the cross-interface transfer of photogenerated electrons, which was the main cause of the depressed photocatalytic hydrogen generation. The reference [32] showed that the photocatalytic hydrogen production performance of pure CdS was 55.84 μmol/g·h, which was close to that of $SrTiO_3$ (51.84 μmol/g·h), while the photocatalytic activity was significantly improved after the carbon fibers, $SrTiO_3$, and CdS were compounded. The above test results showed that the carbon fibers and the oxygen vacancies improved the photocatalytic activity of the CF/$SrTiO_3$ sample, and the coating of CdS on the surface in the later stage significantly enhanced photocatalytic hydrogen evolution of the sample.

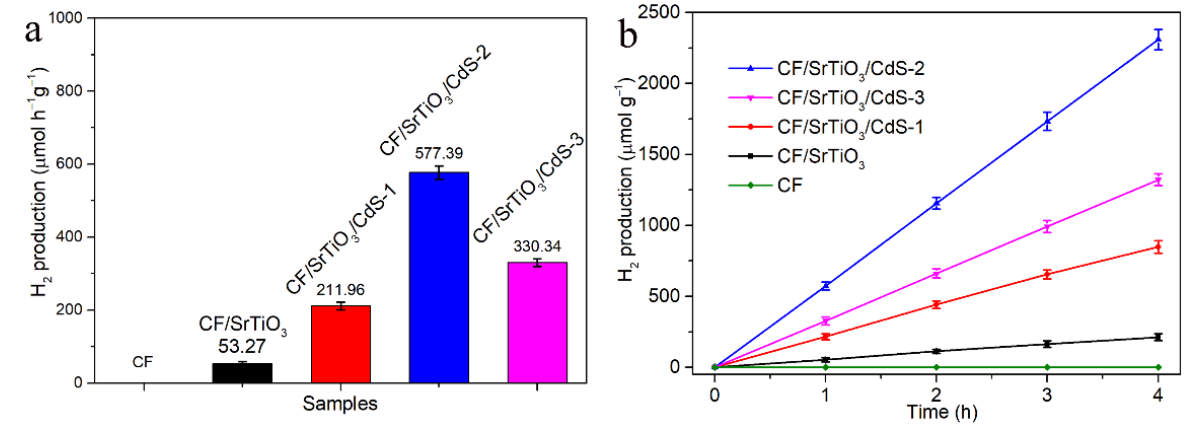

Figure 8. Photocatalytic hydrogen production rates (**a**) and time-dependent hydrogen production amounts (**b**) of different samples.

The stability of the photocatalyst was examined to find out the cost effectiveness of the method by reusing the photocatalyst to its maximum extent [48]. To study the photocatalytic stability of CF/$SrTiO_3$/CdS-2 composite fiber, the cyclic experiment of photocatalytic hydrogen production was carried out, and the test results are shown in Figure 9. After four consecutive cyclic tests of hydrogen production evolution performance, the average photocatalytic hydrogen evolution of the CF/$SrTiO_3$/CdS-2 sample was about 540.39 μmol/g·h. There appeared to be a slight decline over the cyclic experiments, and the test results showed that CF/$SrTiO_3$/CdS-2 maintained relatively stable photocatalytic performance.

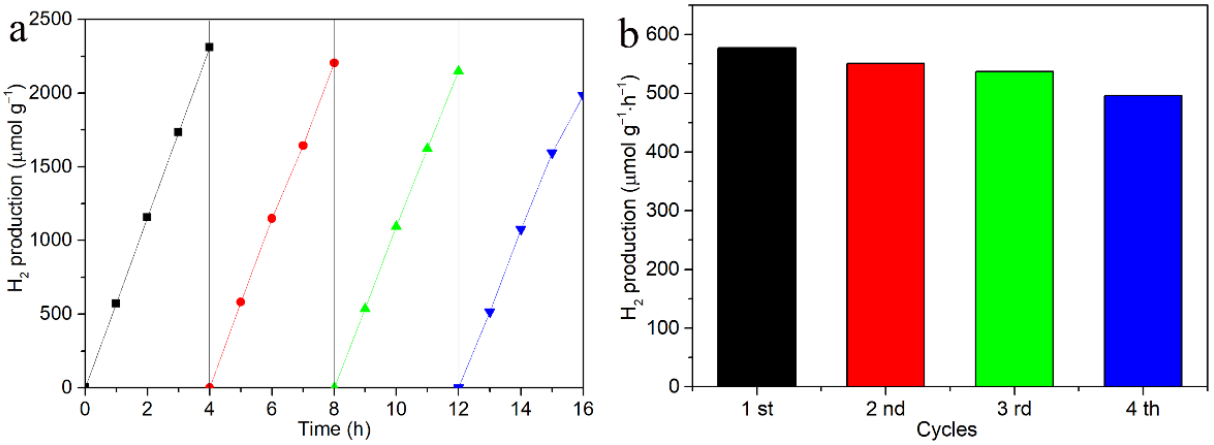

Figure 9. Photocatalytic stability of CF/$SrTiO_3$/CdS-2 composite fiber, (**a**) cycle curve of hydrogen production amount, and (**b**) the corresponding histogram.

The absorption response of catalyst to light was a key factor affecting the photocatalytic performance. The light absorption performances about CF/$SrTiO_3$, CF/$SrTiO_3$/CdS, CF, $SrTiO_3$, and CdS were tested by using a Hitachi F-7000 spectrophotometer. As seen in Figure 10, it could be known from the analysis that the characteristic absorption edge of $SrTiO_3$ was around 375 nm [49], which belongs to ultraviolet light absorption, while the characteristic absorption edge of CdS was around 565 nm, which had a good absorption capacity in the range of visible light. With the introduction of CdS, the light absorption capacity of the composite photocatalytic fiber was improved, which was beneficial to improving the photocatalytic hydrogen production performance.

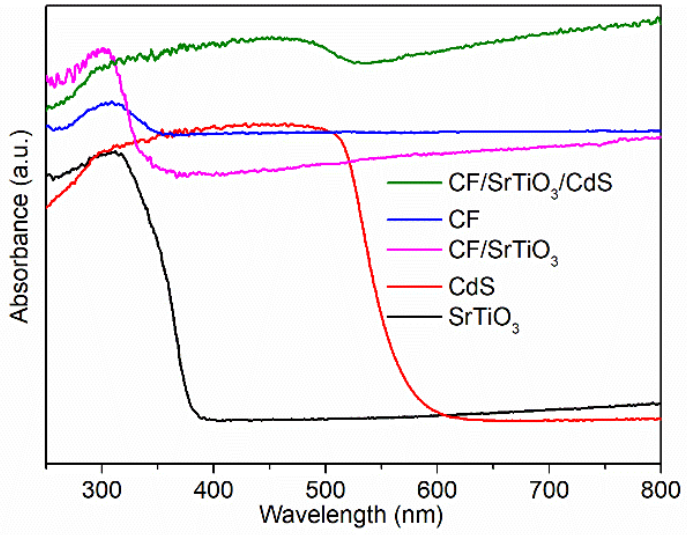

Figure 10. UV–vis diffuse reflection spectra of samples.

Based on Kubelka–Munk theory [50], as shown in Figure 11, it can be obtained that the band gap of CdS alone was about 2.23 eV, and the band gap of pure $SrTiO_3$ was about 3.32 eV.

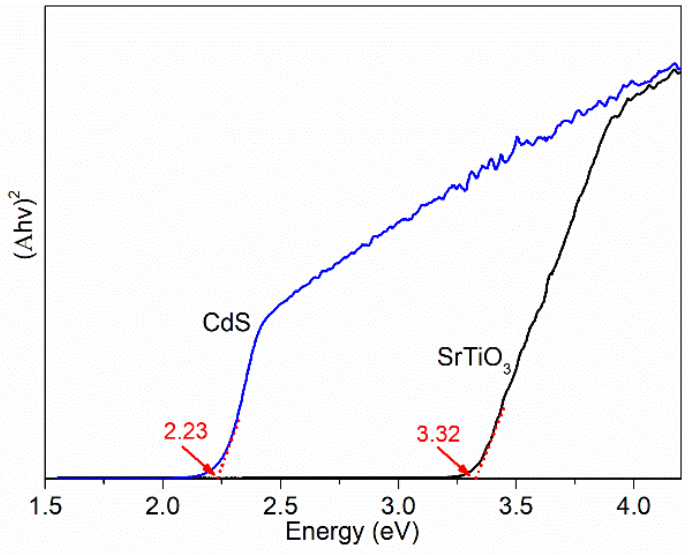

Figure 11. Band gaps of $SrTiO_3$ and CdS.

Based on the Mott–Schottky equation [51], the tangent slopes of the Mott–Schottky spectral lines of $SrTiO_3$ and CdS were positive (Figure 12), indicating that $SrTiO_3$ and CdS were n-type. The flatband potentials about $SrTiO_3$ and CdS were, respectively, −0.69 eV and −0.73 eV (calomel electrode vs. SCE). The potential of aqueous SCE relative to SHE was about 0.24 eV at 25 °C [52], and thus the Fermi levels of $SrTiO_3$ and CdS were, respectively, about –0.45 eV and −0.49 eV. It was generally believed that the conduction band position of the n-type semiconductor was 0.1 eV to the Fermi level [53], so the conduction band positions of $SrTiO_3$ and CdS were, respectively, −0.55 eV and −0.59 eV, and the conduction band position of CdS was higher than that of $SrTiO_3$. The band gaps of $SrTiO_3$ and CdS were, respectively, 3.32 eV and 2.23 eV, as shown in Figure 11. We can deduce that the valence band positions of $SrTiO_3$ and CdS were, respectively, 2.77 eV and 1.64 eV.

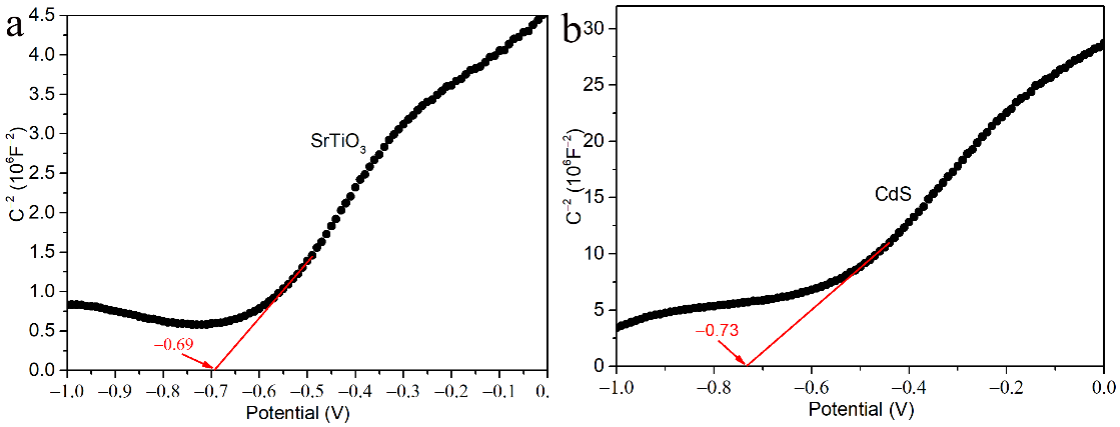

Figure 12. Mott–Schottky plots of samples: (**a**) $SrTiO_3$ and (**b**) CdS.

Carrier separation and migration rates were the main factors affecting the performance of the photocatalyst, and the separation and migration rates of photoelectron–hole pairs could be evaluated by testing the transient photocurrent response and the electrochemical impedance [54,55]. Figure 13 shows the transient photocurrent response spectra and impedance spectra of the photocatalytic materials such as CF/$SrTiO_3$, CF/$SrTiO_3$/CdS-1, CF/$SrTiO_3$/CdS-2, and CF/$SrTiO_3$/CdS-3. As shown in Figure 13a, in the same illumination conditions, the photocurrent of CF/$SrTiO_3$ was about 0.04 μA, while the photocurrent of CF/$SrTiO_3$/CdS-2 was up to 0.23 μA, which was about six times that of CF/$SrTiO_3$. The carbon fiber had no photocurrent response, but it could transfer charges. As for CF/$SrTiO_3$/CdS-2, the substances which had transient photocurrent responses were mainly $SrTiO_3$ and CdS, wherein $SrTiO_3$ mainly absorbed ultraviolet light, and CdS absorbed visible light. The loading of CdS significantly increased the transient photocurrent of the catalyst as well as the generation and separation rates of photoelectron–hole pairs, which was beneficial to improving the photocatalytic hydrogen production performance. Figure 13b shows each of the impedance spectra of CF, CF/$SrTiO_3$, CF/$SrTiO_3$/CdS-1, CF/$SrTiO_3$/CdS-2, and CF/$SrTiO_3$/CdS-3. The high frequency region was composed of an arc, and the radius of the arc reflected the intensity of the charge transfer resistance, as the smaller the radius of the arc was, the higher the migration rate of the carriers would be [56]. Therefore, the photocarrier migration rate of CF/$SrTiO_3$/CdS was higher than that of CF/$SrTiO_3$ and carbon fiber. The above results showed that the separation and migration rates of carriers in the CF/$SrTiO_3$/CdS-2 material was the highest, and that is why the photocatalytic hydrogen production performance was excellent, which was consistent with the results of the photocatalytic hydrogen production experiment shown in Figure 8.

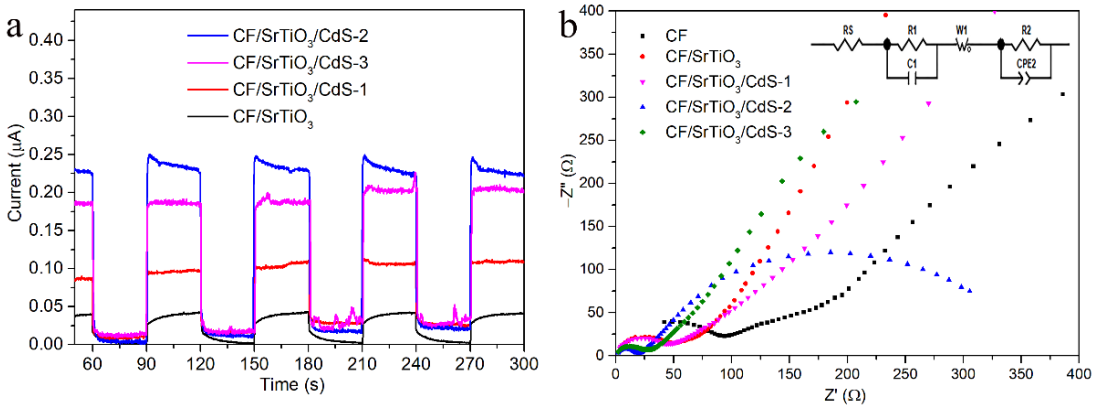

Figure 13. Transient photocurrent response spectra (**a**) and impedance spectra (**b**) of different samples.

To sum up, a photocatalytic hydrogen production mechanism of CF/$SrTiO_3$/CdS was proposed. As shown in Figure 14, the loading of CdS significantly enhanced the visible light absorption capacity of the catalyst and promoted the rapid separation and high-speed migration of photocarriers. Carbon fibers themselves had no hydrogen production performance, and $SrTiO_3$ and CdS alone showed relatively weak HER performances, but the combination of the three showed a relatively strong HER performance. This was because the carbon fibers had a strong electron conduction performance and acted as co-catalysts, CdS had a good absorption performance for visible light, $SrTiO_3$ in the prepared composite catalyst contained abundant oxygen vacancies, and these three factors played a synergistic role in the formation of heterojunctions. As the conduction band position of CdS was higher than that of $SrTiO_3$, photoelectrons migrated from the conduction band position of CdS to the surface of $SrTiO_3$ and then to the carbon fibers. Furthermore, the holes at the valence band position of $SrTiO_3$ migrated to the surface of CdS, thus promoting the fast migration of photocarriers and preventing the recombination of electron–hole pairs. Furthermore, the holes on the $SrTiO_3$ and CdS were easily captured by the sacrificial agents (Na_2S and Na_2SO_3), which promoted the generation and separation of photoelectron–hole pairs and facilitated the hydrogen production of the catalyst.

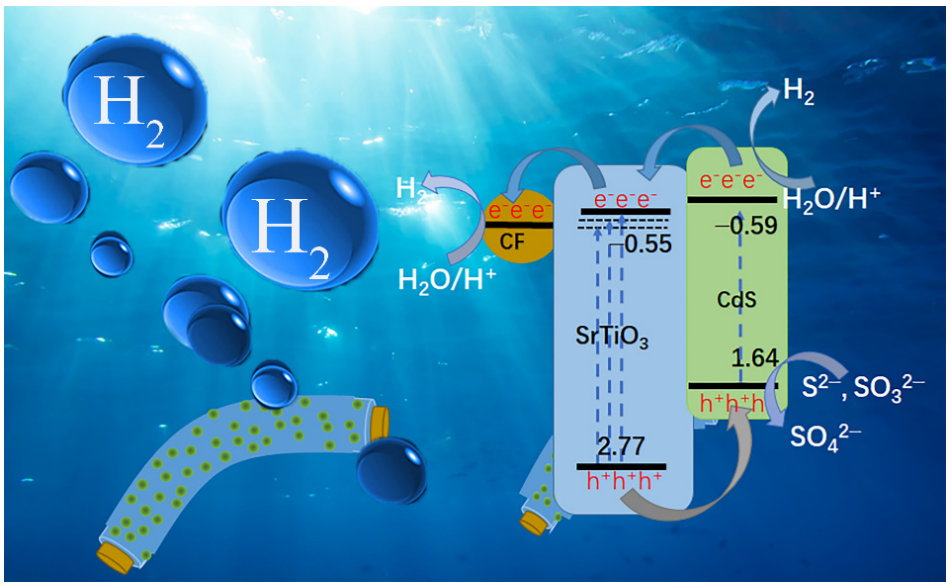

Figure 14. Photocatalytic hydrogen production mechanism of CF/$SrTiO_3$/CdS.

4. Conclusions

In this paper, bamboo pulp fibers were used as precursors of carbon fibers. CF/$SrTiO_3$ composite photocatalytic materials were prepared first by loading and then carbonization, and heterojunctions were formed by loading CdS nanospheres on the surface of the CF/$SrTiO_3$ composite material through the hydrothermal method in order to prepare CF/$SrTiO_3$/CdS with a double-layer core–shell structure. By adjusting the concentration of CdS precursor reagent, the content of CdS in CF/$SrTiO_3$/CdS composite fiber materials was regulated. The photocatalytic hydrogen production experiment showed that the hydrogen production rate of the CF/$SrTiO_3$/CdS-2 sample under the optimized process was as high as 577.39 μmol/g·h, which was about 11 times that of CF/$SrTiO_3$. Carbon fiber itself has no hydrogen production performance, and single $SrTiO_3$ or CdS show relatively weak hydrogen production performance, but this composite photocatalytic material system showed relatively strong photocatalytic hydrogen production performance. The improvement of high photocatalytic hydrogen production performance was mainly attributed to the good light absorption capacity of CdS with a narrow band gap and the formation of excellent heterojunction structures after the composite with $SrTiO_3$, as well as the oxygen vacancy in $SrTiO_3$ and the excellent electrical conductivity of carbon fiber. Carbon fiber

taken as the carrier for CF/$SrTiO_3$/CdS could solve the difficult problem of recycling of traditional $SrTiO_3$- and CdS-dispersed photocatalytic nanomaterials, which is conducive to recycling and improving economic benefits. The preparation methods of CF/$SrTiO_3$ and CF/$SrTiO_3$/CdS materials can also be used in environmental purification, CO_2 reduction, electrocatalysis, and other fields and can also be extended to sensors and other directions.

Author Contributions: Conceptualization, K.-Q.Z. and M.Y.; data curation, Q.H. and J.N.; funding acquisition, J.N. and K.-Q.Z.; Investigation, Q.H. and J.N.; methodology, Q.H. and J.N.; supervision, K.-Q.Z. and M.Y.; writing—original draft, Q.H.; writing—review & editing, Q.H. and K.-Q.Z. All authors have read and agreed to the published version of the manuscript.

Funding: This research was funded by National Key Research and Development Program of China, grant number [2017YFA0204600], and the Qing Lan Project of Jiangsu Province in China.

Institutional Review Board Statement: Not applicable.

Informed Consent Statement: Not applicable.

Data Availability Statement: Data is contained within the article.

Conflicts of Interest: The authors declare no conflict of interest.

References

1. Phoon, B.L.; Lai, C.W.; Juan, J.C.; Show, P.L.; Chen, W.H. A review of synthesis and morphology of $SrTiO_3$ for energy and other applications. *Int. J. Energy Res.* **2019**, *43*, 5151–5174. [CrossRef]
2. Reshak, A. Active photocatalytic water splitting solar-to-hydrogen energy conversion: Chalcogenide photocatalyst Ba_2ZnSe_3 under visible irradiation. *Appl. Catal. B Environ.* **2018**, *221*, 17–26. [CrossRef]
3. Cui, J.; Yang, X.; Yang, Z.; Sun, Y.; Chen, X.; Liu, X.; Wang, D.; Jiang, S.; Liu, L.; Ye, J. Zr–Al co-doped $SrTiO_3$ with suppressed charge recombination for efficient photocatalytic overall water splitting. *Chem. Commun.* **2021**, *57*, 10640–10643. [CrossRef] [PubMed]
4. Cui, Y.; Sun, H.; Guo, P. Highly efficient $SrTiO_3$/Ag_2O np heterojunction photocatalysts: Improved charge carrier separation and enhanced visible-light harvesting. *Nanotechnology* **2020**, *31*, 245702. [CrossRef] [PubMed]
5. Tan, C.-E.; Lee, J.-T.; Su, E.-C.; Wey, M.-Y. Facile approach for Z-scheme type Pt/g-C_3N_4/$SrTiO_3$ heterojunction semiconductor synthesis via low-temperature process for simultaneous dyes degradation and hydrogen production. *Int. J. Hydrogen Energy* **2020**, *45*, 13330–13339. [CrossRef]
6. Xie, L.; Ai, Z.; Zhang, M.; Sun, R.; Zhao, W. Enhanced hydrogen evolution in the presence of plasmonic Au-photo-sensitized g-C3N4 with an extended absorption spectrum from 460 to 640 nm. *PLoS ONE* **2016**, *11*, e0161397. [CrossRef]
7. Wang, G.; Ling, Y.; Li, Y. Oxygen-deficient metal oxide nanostructures for photoelectrochemical water oxidation and other applications. *Nanoscale* **2012**, *4*, 6682–6691. [CrossRef]
8. Khamkhash, L.; Em, S.; Molkenova, A.; Hwang, Y.-H.; Atabaev, T.S. Crack-Free and Thickness-Controllable Deposition of TiO_2–rGO Thin Films for Solar Harnessing Devices. *Coatings* **2022**, *12*, 218. [CrossRef]
9. Low, J.; Yu, J.; Jaroniec, M.; Wageh, S.; Al-Ghamdi, A.A. Heterojunction photocatalysts. *Adv. Mater.* **2017**, *29*, 1601694. [CrossRef]
10. Feng, C.; Chen, Z.; Hou, J.; Li, J.; Li, X.; Xu, L.; Sun, M.; Zeng, R. Effectively enhanced photocatalytic hydrogen production performance of one-pot synthesized MoS_2 clusters/CdS nanorod heterojunction material under visible light. *Chem. Eng. J.* **2018**, *345*, 404–413. [CrossRef]
11. Yuan, M.; Zhou, W.-H.; Kou, D.-X.; Zhou, Z.-J.; Meng, Y.-N.; Wu, S.-X. Cu_2ZnSnS_4 decorated CdS nanorods for enhanced visible-light-driven photocatalytic hydrogen production. *Int. J. Hydrogen Energy* **2018**, *43*, 20408–20416. [CrossRef]
12. Wei, Z.; Zhou, Z.; Yang, M.; Lin, C.; Zhao, Z.; Huang, D.; Chen, Z.; Gao, J. Multifunctional Ag@ Fe_2O_3 yolk–shell nanoparticles for simultaneous capture, kill, and removal of pathogen. *J. Mater. Chem.* **2011**, *21*, 16344–16348. [CrossRef]
13. Pinchetti, V.; Meinardi, F.; Camellini, A.; Sirigu, G.; Christodoulou, S.; Bae, W.K.; De Donato, F.; Manna, L.; Zavelani-Rossi, M.; Moreels, I. Effect of core/shell interface on carrier dynamics and optical gain properties of dual-color emitting CdSe/CdS nanocrystals. *ACS Nano* **2016**, *10*, 6877–6887. [CrossRef]
14. Wu, H.-L.; Sato, R.; Yamaguchi, A.; Kimura, M.; Haruta, M.; Kurata, H.; Teranishi, T. Formation of pseudomorphic nanocages from Cu_2O nanocrystals through anion exchange reactions. *Science* **2016**, *351*, 1306–1310. [CrossRef] [PubMed]
15. Ma, L.; Chen, K.; Nan, F.; Wang, J.H.; Yang, D.J.; Zhou, L.; Wang, Q.Q. Improved Hydrogen Production of Au–Pt–CdS Hetero-Nanostructures by Efficient Plasmon-Induced Multipathway Electron Transfer. *Adv. Funct. Mater.* **2016**, *26*, 6076–6083. [CrossRef]
16. Lei, S.-L.; Yu, J.; Bao, S.-K.; Zeng, G.-S.; Liu, H.-L.; Wu, D.-D.; Tang, X.-H.; Zou, J.-P.; Au, C.-T. High-performance heterostructured CdS/$Ba_{1-x}Sr_xTiO_3$ system with unique synergism for photocatalytic H_2 evolution. *Appl. Catal. A Gen.* **2015**, *493*, 58–67. [CrossRef]

17. Yuan, W.; Zhang, Z.; Cui, X.; Liu, H.; Tai, C.; Song, Y. Fabrication of hollow mesoporous CdS@ TiO_2@ Au microspheres with high photocatalytic activity for hydrogen evolution from water under visible light. *ACS Sustain. Chem. Eng.* **2018**, *6*, 13766–13777. [CrossRef]
18. Shen, R.; Ren, D.; Ding, Y.; Guan, Y.; Ng, Y.H.; Zhang, P.; Li, X. Nanostructured CdS for efficient photocatalytic H_2 evolution: A review. *Sci. China Mater.* **2020**, *63*, 2153–2188. [CrossRef]
19. Wu, G.; Xiao, L.; Gu, W.; Shi, W.; Jiang, D.; Liu, C. Fabrication and excellent visible-light-driven photodegradation activity for antibiotics of $SrTiO_3$ nanocube coated CdS microsphere heterojunctions. *RSC Adv.* **2016**, *6*, 19878–19886. [CrossRef]
20. Huang, L.; Wei, Z.; Ma, L.; Zhang, F.; Wu, X. Growth of cubic CdS films on TiO_2-terminated (100) $SrTiO_3$ substrate. *Mater. Chem. Phys.* **2016**, *183*, 334–338. [CrossRef]
21. Lei, Y.; Xu, J.; Li, R.; Chen, F. Solvothermal synthesis of CdS–graphene composites by varying the Cd/S ratio. *Ceram. Int.* **2015**, *41*, 3158–3161. [CrossRef]
22. Manchala, S.; Gandamalla, A.; Rao, V.N.; Venkatakrishnan, S.M.; Shanker, V. Solar-light responsive efficient H_2 evolution using a novel ternary hierarchical $SrTiO_3$/CdS/carbon nanospheres photocatalytic system. *J. Nanostruct. Chem.* **2022**, *12*, 179–191. [CrossRef]
23. Li, H.; Pan, J.; Zhao, W.; Li, C. The 2D nickel-molybdenum bimetals sulfide synergistic modified hollow cubic CdS towards enhanced photocatalytic water splitting hydrogen production. *Appl. Surf. Sci.* **2019**, *497*, 143769. [CrossRef]
24. Li, X.; Deng, Y.; Jiang, Z.; Shen, R.; Xie, J.; Liu, W.; Chen, X. Photocatalytic hydrogen production over CdS nanomaterials: An interdisciplinary experiment for introducing undergraduate students to photocatalysis and analytical chemistry. *J. Chem. Educ.* **2019**, *96*, 1224–1229. [CrossRef]
25. Quan, H.; Qian, K.; Xuan, Y.; Lou, L.-L.; Yu, K.; Liu, S. Superior performance in visible-light-driven hydrogen evolution reaction of three-dimensionally ordered macroporous $SrTiO_3$ decorated with $Zn_xCd_{1-x}S$. *Front. Chem. Sci. Eng.* **2021**, *15*, 1561–1571. [CrossRef]
26. Park, D.; Ju, H.; Kim, J. Effect of $SrTiO_3$ nanoparticles in conductive polymer on the thermoelectric performance for efficient thermoelectrics. *Polymers* **2020**, *12*, 777. [CrossRef]
27. Han, B.; Wu, L.; Li, J.; Wang, X.; Peng, Q.; Wang, N.; Li, X. A nanoreactor based on $SrTiO_3$ coupled TiO_2 nanotubes confined Au nanoparticles for photocatalytic hydrogen evolution. *Int. J. Hydrogen Energy* **2020**, *45*, 1559–1568. [CrossRef]
28. Liu, B.; Du, C.; Chen, J.; Zhai, J.; Wang, Y.; Li, H. Preparation of well-developed mesoporous activated carbon fibers from plant pulp fibers and its adsorption of methylene blue from solution. *Chem. Phys. Lett.* **2021**, *771*, 138535. [CrossRef]
29. Lam, S.S.; Azwar, E.; Peng, W.; Tsang, Y.F.; Ma, N.L.; Liu, Z.; Park, Y.-K.; Kwon, E.E. Cleaner conversion of bamboo into carbon fibre with favourable physicochemical and capacitive properties via microwave pyrolysis combining with solvent extraction and chemical impregnation. *J. Clean. Prod.* **2019**, *236*, 117692. [CrossRef]
30. Luo, X.; Ke, Y.; Yu, L.; Wang, Y.; Homewood, K.P.; Chen, X.; Gao, Y. Tandem CdS/TiO_2 (B) nanosheet photocatalysts for enhanced H_2 evolution. *Appl. Surf. Sci.* **2020**, *515*, 145970. [CrossRef]
31. Dong, Y.; Zhu, X.; Pan, F.; Deng, B.; Liu, Z.; Zhang, X.; Huang, C.; Xiang, Z.; Lu, W. Mace-like carbon fiber/ZnO nanorod composite derived from typha orientalis for lightweight and high-efficient electromagnetic wave absorber. *Adv. Compos. Hybrid Mater.* **2021**, *4*, 1002–1014. [CrossRef]
32. Vu, C.M.; Nguyen, D.D.; Sinh, L.H.; Choi, H.J.; Pham, T.D. Micro-fibril cellulose as a filler for glass fiber reinforced unsaturated polyester composites: Fabrication and mechanical characteristics. *Macromol. Res.* **2018**, *26*, 54–60. [CrossRef]
33. Liu, Y.; Chen, Y.; Chen, Z.; Qi, H. A novel cellulose-derived carbon aerogel@ $Na_2Ti_3O_7$ composite for efficient photocatalytic degradation of methylene blue. *J. Appl. Polym. Sci.* **2021**, *138*, 51347. [CrossRef]
34. Wan, S.; Chen, M.; Ou, M.; Zhong, Q. Plasmonic Ag nanoparticles decorated $SrTiO_3$ nanocubes for enhanced photocatalytic CO_2 reduction and H_2 evolution under visible light irradiation. *J. CO2 Util.* **2019**, *33*, 357–364. [CrossRef]
35. Deng, Y.; Shu, S.; Fang, N.; Wang, R.; Chu, Y.; Liu, Z.; Cen, W. One-pot synthesis of $SrTiO_3$-$SrCO_3$ heterojunction with strong interfacial electronic interaction as a novel photocatalyst for water splitting to generate H_2. *Chin. Chem. Lett.* **2022**. [CrossRef]
36. Huang, Y.; Yu, Y.; Yu, Y.; Zhang, B. Oxygen vacancy engineering in photocatalysis. *Sol. RRL* **2020**, *4*, 2000037. [CrossRef]
37. Fan, Y.; Liu, Y.; Cui, H.; Wang, W.; Shang, Q.; Shi, X.; Cui, G.; Tang, B. Photocatalytic Overall Water Splitting by $SrTiO_3$ with Surface Oxygen Vacancies. *Nanomaterials* **2020**, *10*, 2572. [CrossRef]
38. Al Marzouqi, F.; Kim, Y.; Selvaraj, R. Shifting of the band edge and investigation of charge carrier pathways in the CdS/gC_3N_4 heterostructure for enhanced photocatalytic degradation of levofloxacin. *New J. Chem.* **2019**, *43*, 9784–9792. [CrossRef]
39. Pan, B.; Qin, J.; Wang, X.; Su, W. Efficient self-assembly synthesis of $LaPO_4$/CdS hierarchical heterostructure with enhanced visible-light photocatalytic CO_2 reduction. *Appl. Surf. Sci.* **2020**, *504*, 144379. [CrossRef]
40. Li, C.-Q.; Yi, S.-S.; Chen, D.-L.; Liu, Y.; Li, Y.-J.; Lu, S.-Y.; Yue, X.-Z.; Liu, Z.-Y. Oxygen vacancy engineered $SrTiO_3$ nanofibers for enhanced photocatalytic H_2 production. *J. Mater. Chem. A* **2019**, *7*, 17974–17980. [CrossRef]
41. Peng, S.; Gan, C.; Yang, Y.; Ji, S.; Li, Y. Low Temperature and Controllable Formation of Oxygen Vacancy $SrTiO_{3-x}$ by Loading Pt for Enhanced Photocatalytic Hydrogen Evolution. *Energy Technol.* **2018**, *6*, 2166–2171. [CrossRef]
42. Albiss, B.; Abu-Dalo, M. Photocatalytic degradation of methylene blue using zinc oxide nanorods grown on activated carbon fibers. *Sustainability* **2021**, *13*, 4729. [CrossRef]
43. Liu, R.; Li, W.; Peng, A. A facile preparation of TiO_2/ACF with CTi bond and abundant hydroxyls and its enhanced photocatalytic activity for formaldehyde removal. *Appl. Surf. Sci.* **2018**, *427*, 608–616. [CrossRef]

44. Pan, J.; Liu, Y.; Ou, W.; Li, S.; Li, H.; Wang, J.; Song, C.; Zheng, Y.; Li, C. The photocatalytic hydrogen evolution enhancement of the MoS_2 lamellas modified g-C_3N_4/$SrTiO_3$ core-shell heterojunction. *Renew. Energy* **2020**, *161*, 340–349. [CrossRef]
45. Zhang, X.; Cheng, Z.; Deng, P.; Zhang, L.; Hou, Y. $NiSe_2$/$Cd_{0.5}Zn_{0.5}S$ as a type-II heterojunction photocatalyst for enhanced photocatalytic hydrogen evolution. *Int. J. Hydrogen Energy* **2021**, *46*, 15389–15397. [CrossRef]
46. Nagakawa, H.; Nagata, M. Elucidating the Factors Affecting Hydrogen Production Activity Using a CdS/TiO_2 Type-II Composite Photocatalyst. *ACS Omega* **2021**, *6*, 4395–4400. [CrossRef] [PubMed]
47. Zhao, J.; Yang, H.; Li, Y.; Lu, K. Photocatalytic activity of CdS nanoparticles enhanced by the interaction between piezotronic effect and phase junction. *J. Alloys Compd.* **2020**, *815*, 152494. [CrossRef]
48. Kumar, P.S.; Selvakumar, M.; Babu, S.G.; Induja, S.; Karuthapandian, S. CuO/ZnO nanorods: An affordable efficient pn heterojunction and morphology dependent photocatalytic activity against organic contaminants. *J. Alloys Compd.* **2017**, *701*, 562–573. [CrossRef]
49. Kiran, K.; Ashwath Narayana, B.; Lokesh, S. Enhanced photocatalytic activity of perovskite $SrTiO_3$ nanorods. *Solid State Technol.* **2020**, *63*, 1913–1920.
50. He, C.; Deng, C.; Wang, J.; Gu, X.; Wu, T.; Zhu, K.; Liu, Y. Crystal orientation dependent optical transmittance and band gap of $Na_{0.5}Bi_{0.5}TiO_3$–$BaTiO_3$ single crystals. *Phys. B Condens. Matter* **2016**, *483*, 44–47. [CrossRef]
51. Honorio, L.M.C.; de Oliveira, A.L.M.; da Silva Filho, E.C.; Osajima, J.A.; Hakki, A.; Macphee, D.E.; dos Santos, I.M.G. Supporting the photocatalysts on ZrO_2: An effective way to enhance the photocatalytic activity of $SrSnO_3$. *Appl. Surf. Sci.* **2020**, *528*, 146991. [CrossRef]
52. Gong, H.; Zhang, X.; Wang, G.; Liu, Y.; Li, Y.; Jin, Z. Dodecahedron ZIF-67 anchoring ZnCdS particles for photocatalytic hydrogen evolution. *Mol. Catal.* **2020**, *485*, 110832. [CrossRef]
53. Wang, Y.; Zeng, Y.; Chen, X.; Wang, Q.; Guo, L.; Zhang, S.; Zhong, Q. One-step hydrothermal synthesis of a novel 3D $BiFeWO_x$/Bi_2WO_6 composite with superior visible-light photocatalytic activity. *Green Chem.* **2018**, *20*, 3014–3023. [CrossRef]
54. Su, S.-F.; Ye, L.-M.; Tian, Q.-M.; Situ, W.-B.; Song, X.-L.; Ye, S.-Y. Photoelectrocatalytic inactivation of Penicillium expansum spores on a Pt decorated TiO_2/activated carbon fiber photoelectrode in an all-solid-state photoelectrochemical cell. *Appl. Surf. Sci.* **2020**, *515*, 145964. [CrossRef]
55. Zhu, Y.-C.; Xu, Y.-T.; Xue, Y.; Fan, G.-C.; Zhang, P.-K.; Zhao, W.-W.; Xu, J.-J.; Chen, H.-Y. Three-dimensional CdS@ carbon fiber networks: Innovative synthesis and application as a general platform for photoelectrochemical bioanalysis. *Anal. Chem.* **2019**, *91*, 6419–6423. [CrossRef]
56. Shi, Z.; Xu, P.; Shen, X.; Zhang, Y.; Luo, L.; Duoerkun, G.; Zhang, L. TiO_2/MoS_2 heterojunctions-decorated carbon fibers with broad-spectrum response as weaveable photocatalyst/photoelectrode. *Mater. Res. Bull.* **2019**, *112*, 354–362. [CrossRef]